# Analytical Methods

Accepted Manuscript

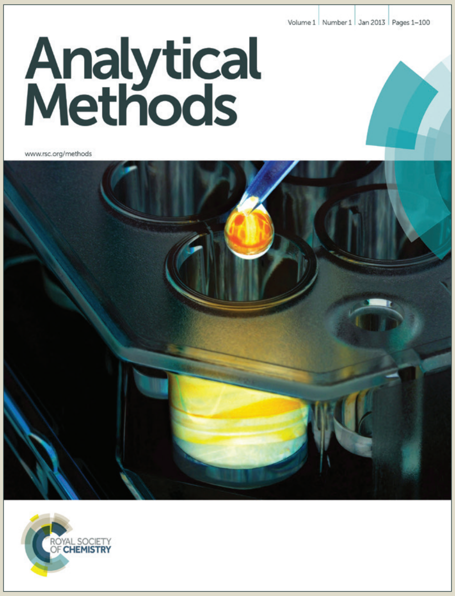

ROYAL SOCIETY
OF CHEMISTRY

www.rsc.org/methods

# Table of contents entry

## Color Image

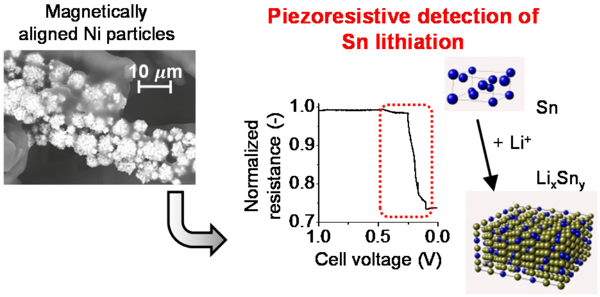

## Text highlight

Strain from Li-alloying anodes *in operando* is directly detected using generic battery components as a piezoresistive sensor. Magnetic-field alignment effectively enhances the sensitivity of this sensor.

Journal Name RSCPublishing

ARTICLE

Cite this: DOI: 10.1039/x0xx00000x

# Magnetically tuneable piezoresistive sensor for direct, *in situ* strain measurement in Li-ion batteries

J. Matthew Kaule,[a] Lance R. Hoffman,[b] and Hitomi Mukaibo*[ab]

Received 00th January 2012,
Accepted 00th January 2012

DOI: 10.1039/x0xx00000x

**www.rsc.org/**

This paper demonstrates the first example of using generic Li-ion battery components (Nickel, carboxymethylcellulose and styrene-butadiene rubber) to prepare piezoresistive materials (PRM) that detect strain of lithiating Sn *in operando*. The PRM was prepared by mixing the three components and molding it into the desired shape. Three different types of Ni microparticle arrangement strategies were investigated to study their effects on piezoresistive performance: an alignment parallel to or perpendicular to the direction of strain, and no alignment (control, random dispersion). The alignment was directed by an external magnetic field during sample preparation, and confirmed using cross-sectional SEM images. Significant differences were found between the different alignments, with the parallel alignment resulting in the lowest percolation threshold of 4 vol % Ni and perpendicular alignment the highest of 11 vol % Ni. For a fixed fraction of Ni microparticles at 4 vol %, the difference in alignment resulted in a difference in the gauge factor by three orders of magnitude. The stress-strain curve of the prepared PRMs showed a typical response seen for porous structures, which was consistent with the SEM images. The PRM samples are compatible with the low operating potential and the organic Li-ion electrolyte, and its porous structure allows electrolyte infusion that ensures ionic conductivity of the material. Lithiation of Sn was successfully detected as a change in resistance using a parallel-aligned PRM with no additional treatment. The method described here offers significant merits over conventional approaches: the ability to directly monitor strain without complex modelling, the simple low cost setup that does not require specialized equipment, and the ability to easily control the PRM performance by magnetically directed assembly.

## Introduction

Li-ion battery is a key energy technology to support the demands of hybrid electrical vehicles, electricity consumption and portable electronic devices.[1, 2] Metals and semiconductors that alloy with lithium are promising alternatives to conventional Li-intercalating anodes, due to their extremely high energy density.[3] The most prominent drawback for such materials is their drastic volume change induced by their reaction with Li-ions during battery operation. The volume change results in stress, cracking, and loss of mechanical integrity that strongly deteriorates the battery performance. Direct measurement of the volume change during operation can help to understand its reaction mechanism, reveal critical information on the battery performance, and lead to better design and optimization of the alloying anodes.[4] Previous reports for such measurements include digital image correlation (DIC) analysis,[5-8] dilatometry,[9-11] electrochemical strain microscopy (ESM),[12] *in situ* atomic force microscopy (AFM),[13-16] *in situ* transmission electron microscopy (TEM) [17-19], and *in situ* X-ray transmission microscopy[20]. All of these sophisticated approaches have been demonstrated to be effective and insightful, but they require extensive instrumentation and expertise. This makes it challenging, if not impossible, for their application to the broad Li-ion battery community.

The objective of this paper is to demonstrate a simple, generic technique for detecting lithiation-induced strain by: (1) preparing composite piezoresistive material (PRM) with conventional Li-ion battery elements and (2) tuning the sensitivity of the PRM through magnetic alignment. “Composite PRM” is a widely used term that indicates a material with electrically conducting particles (or fillers) dispersed within an insulating polymer matrix.[21] Percolation and quantum tunnelling is a well-accepted mechanism for the conductivity within such composite materials.[21, 22] When strain is applied, material deformation changes the distance between the conductive particles, which results in a measureable change in electric resistance. Composite PRMs have gained interest for numerous applications including magnetorheological elastomers[23-25], stretchable/transparent electrodes[26, 27] adhesives[28], tactile sensors,[21] and material fatigue sensing.[29] Although a random mixture of all components is the most common configuration of composite PRM, aligning the conductive particles (also known as directed assembly) has been reported to be effective in improving the PRM performance.[30] This is because conductive particles are at a much closer proximity after the alignment, which results in a reduced percolation threshold and higher sensitivity to applied strain. Previous reports have used tensile strain,[31] electric fields,[32] template array,[33] and magnetic fields[25-27, 34] to align the conductive particles and modify PRM performance.

We show here for the first time that conventional elements used in Li-ion batteries, *i.e.,* Ni microparticles (current collector), carboxymethylcellulose (binder), and styrene-butadiene rubber (binder), can be applied to prepare a composite PRM that detects the volume expansion of electrochemically lithiated Sn electrode. Furthermore, we show that the sensitivity and the dynamic sensing range of our PRM sample can be easily tuned by controlling the alignment of the Ni microparticles using an external magnetic field during sample preparation.

## Experimental

### Chemicals and materials

Chemicals and materials were purchased from the following suppliers and used as received: carboxymethylcellulose (CMC) and styrene-butadiene rubber (SBR) from MTI Corporation (Richmond, USA); nickel microparticles (Ni MPs, 3–7 μm) from Alfa Aesar (Ward Hill, USA), and *N,N*-dimethylformamide (DMF) from Fisher Scientific (Pittsburgh, USA). Peel-A-Way disposable embedding molds S-22 were purchased from Polysciences, Inc. (Warrington, USA). Electrolyte consisting of 1 M $LiClO_4$ in ethylene carbonate (EC) and propylene carbonate (PC) (1:1 vol %) was used as purchased from BASF (Florham Park, USA). A porous separator was cut from a polycarbonate membrane (1.2 μm pores) purchased from Millipore (Billerica, USA). The following materials were used after polishing their surfaces to remove any oxides and contaminants: 2 mm-thick Sn foil (99.9985%) purchased from Alfa Aesar (Ward Hill, USA), Li foil (99.9%) purchased from Fisher Scientific (Pittsburgh, USA), and Type 304 stainless steel mesh (s.s. mesh) purchased from McMaster-Carr (Cleveland, USA).

### PRM preparation

**ALIGNED SAMPLE.** PRM composite slurry was prepared by weighing the Ni MPs, CMC, and SBR to the desired weight percentage, and then mixing thoroughly with DMF until a slurry with uniform consistency was obtained. A mold was prepared by cutting the commercial plastic mold to remove the bottom surface and adjust the height to 8 mm. The mold was placed on an electromagnet purchased from Magnetech Corp. (Novi, USA; Part#: OP-1212) covered with plastic wrap, and the PRM composite slurry was poured into the mold. The mold was then capped by another electromagnet, also covered with plastic wrap, and a current of 0.702 A was applied to both electromagnets using two DC power supplies (Model 9312-PS; MPJA, Lake Park, USA) for 1 h. This produces a magnetic flux of 250 Gauss at the magnet poles' surface. Following this step, the mold with the PRM slurry was placed onto a glass slide and heated in an oven overnight at 120 °C to remove residual DMF. After the sample cooled, the mold was carefully peeled away from the sample. Perpendicular and parallel aligned PRM samples were prepared identically, but rotated 90° from one another before testing.

**CONTROL SAMPLE (NO ALIGNMENT).** The PRM composite slurry and the mold were prepared as described above. The slurry was poured into the mold and sandwiched between two plastic wrap covered glass slides for 1 h at room temperature. The top glass slide was then removed and the sample was heated in an oven overnight at 120 °C to remove residual DMF. After the sample cooled, the mold was carefully peeled away from the sample.

### PRM characterization

**ALIGNMENT OF NI MPS.** Samples with 33 wt % Ni MPs were prepared for imaging cross-sectional morphology. The backscatter detector of the field emission scanning electron microscopy (FE-SEM) (Zeiss Auriga CrossBeam SEM-FIB) was used. The samples were immersed in liquid nitrogen and then snapped through their thickness around their centerline. The broken samples were fixed onto the SEM stub using double-sided carbon tape, such that their cross-sectional surface faced the SEM detector. Sufficient electrical contact between the stub and the sample surface was achieved using carbon black paste and gold sputtering (60 Å thick).

**NATIVE RESISTIVITY MEASUREMENT.** The term "native" resistivity is used to indicate the resistivity measured without any compression (zero load). The PRM sample was sandwiched between two flat brass plates that were connected to a multimeter. Resistivity, $\rho\ [\Omega \cdot \mathrm{mm}]$, was calculated from the measured resistance, with respect to the distance between the plates (*i.e.,* the thickness of the sample, 8 mm) and the contact area between the sample and the plates (100 $mm^2$). The volume fraction of Ni in each sample, $f_V$, was determined by:

$$f_V = \frac{\rho_{\mathrm{sample}}}{\rho_{\mathrm{Ni}}} f_m$$

where $\rho_{\mathrm{sample}}$ is the bulk density of each sample (calculated from the mass and volume of the samples), $\rho_{\mathrm{Ni}}$ is the density of metallic Ni (8.908 $g/cm^3$),[35] and $f_m$ is the mass fraction of Ni in each sample.

**STRESS *VS.* RESISTANCE MEASUREMENT.** PRM samples with 33 wt % Ni MPs were infiltrated with 1 M $LiClO_4$/EC + PC electrolyte under 100 kPa for 20 h at room temperature to ensure consistency with the anode testing experiments. The relationship between sample resistance and applied stress was studied using custom platens on an MTS Criterion Universal Testing System (Eden Prairie, USA). Figure 1 illustrates the setup used here. A brass plate with 2 wires soldered to its surface was embedded in a cylindrical insulating resin, sized to match standard MTS platens. The custom platens were screwed to the top and the bottom MTS mounts, and the sample was sandwiched between the metallic surfaces of the custom platens. The MTS applied a compressive strain to the sample at 0.25 mm/min, and recorded the change in stress with strain data at 5 Hz. Simultaneously, a Model 5492B bench-top multimeter from BK Precision (Yorba Linda, USA) was used in a 4-probe configuration to record the change in resistance with time data at 5 Hz. Data from MTS and the multimeter were combined to yield the stress *vs.* resistance relationship of each sample. Normalized resistance, $\Delta R/R_0$, was calculated by the following equation:

$$\frac{\Delta R}{R_0} = \frac{R_c - R_0}{R_0}$$

where $R_0$ and $R_C$ are the resistances of the PRM sample before and after compression, respectively.

Table 1 Sample dimensions and Ni MP concentration.

| $f_m$ (wt %) | $\rho$ (g/cm$^3$) | $f_v$ (vol %) |
|---|---|---|
| **33** | 1.10 | 4.08 |
| **50** | 1.45 | 8.16 |
| **60** | 1.64 | 11.0 |
| **67** | 1.38 | 12.6 |
| **71** | 1.86 | 14.9 |

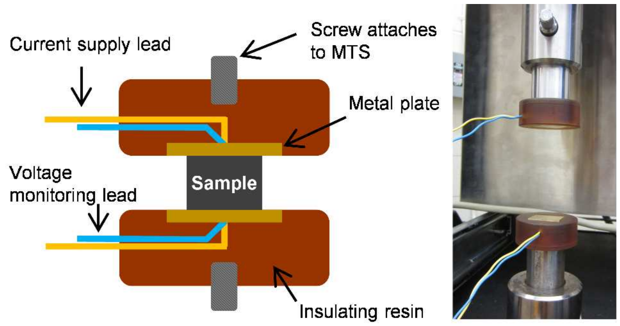

**Fig. 1** Custom platens for simultaneous monitoring of resistance, stress and strain as the sample is being compressed by MTS. The photograph shows the MTS set-up with custom platens. The electric leads from the platens were connected to a digital multimeter (not shown).

***IN SITU* STRAIN TESTING.** All lithiation/delithiation experiments were done in an inert argon atmosphere within an MB 200B glove box (MBRAUN, Stratham, USA). PRM samples were infiltrated with 1 M LiClO$_4$/EC + PC electrolyte under 100 kPa for 20 h at room temperature, and assembled in a custom device made of Teflon®, shown in Fig. 2. There were 7 layers of components in this device: (1) Cu current collector (lead 1), (2) Sn working electrode, (3) PC-membrane separators (six layers, infiltrated with electrolyte at 100 kPa, 30 min), (4) s.s. mesh lead (lead 3), (5) PRM, (6) Li counter electrode and (7) another Cu current collector (lead 2). The PRM was sandwiched between the s.s. mesh and Li foil such that the magnetic alignment of the Ni MPs was normal to the Sn foil surface. A set screw was used for applying minimal pressure between the layers and to ensure sufficient contact. After assembling the layers, an additional 1 mL of electrolyte was added to the device to prevent drying.

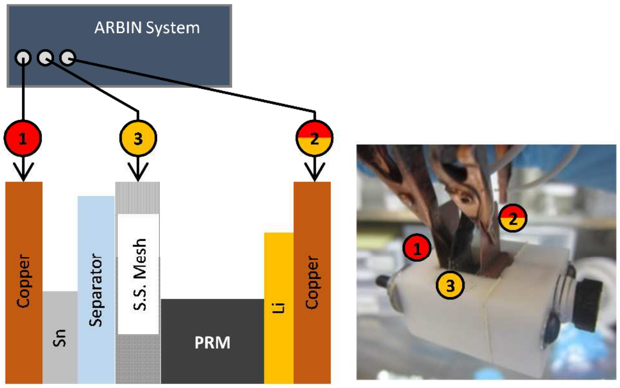

**Fig. 2** Device setup for measuring the change in PRM resistance during lithiation/delithiation of the Sn electrode. The photograph shows the Li-Sn half-cell assembly.

Sn was lithiated/delithiated at a constant current of 0.5 mA/g Sn using a Model BT2043 battery cycler from ARBIN Instruments (College Station, USA). Sn was lithiated from its open circuit voltage to 0.01 V. The change in voltage between leads 2 and 3 during Sn lithiation/delithiation was measured using the auxiliary voltage monitoring probe of the ARBIN system. Since our sample is confirmed to show ohmic response,[36] the measured change in voltage was used to calculate the resistance of PRM ($R = E/I$ ).

## Results and discussion

### Alignment of Ni MPs

Figure 3a and 3b shows FE-SEM images of the cross-sectional morphology of the PRM samples. The samples were imaged with a backscatter detector to enhance the contrast between the metallic Ni MPs and the organic CMC/SBR binder. The Ni MPs were dispersed as aggregates within the porous macro-structure of the binder. The porous nature of the binder is important for the following battery anode experiments, for it allows penetration of electrolyte and ensures Li-ion conductivity. When the samples were prepared without application of the magnetic field (Fig. 3a), the aggregates were scattered randomly throughout the binder matrix, similar to what has been reported for metal microparticles dispersed in a homogeneous polymer matrix.[27, 28, 37-39] On the other hand, when the samples were prepared under the influence of the magnetic field (Fig. 3b), we observed regions where Ni MPs anisotropically aligned as linear aggregates along the magnetic field line (Fig. 3b inset). The binder material surrounding the Ni MPs (appearing semi-translucent in the SEM image) is expected to help maintain the alignment of the aggregates after the magnetic field is removed from the sample. Although not studied here, maintaining external magnetic field until the binder fully solidifies is expected to improve the reproducibility of the aligned aggregate structure. The length of the aggregates depends on the volume fraction of the Ni MPs, and is expected to become longer with higher Ni MPs content.[27]

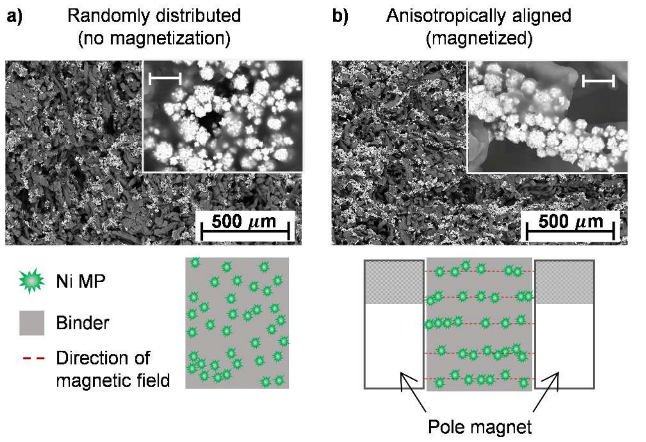

**Fig. 3** Cross-sectional FE-SEM images and schematic illustrations of the PRM prepared (a) without and (b) with application of magnetic field. The insets show the zoomed-in images of the Ni MP aggregates embedded within the binder. The scale bar for both insets are 10 µm. The dotted line indicates the direction of the magnetic field that was present during the sample preparation.

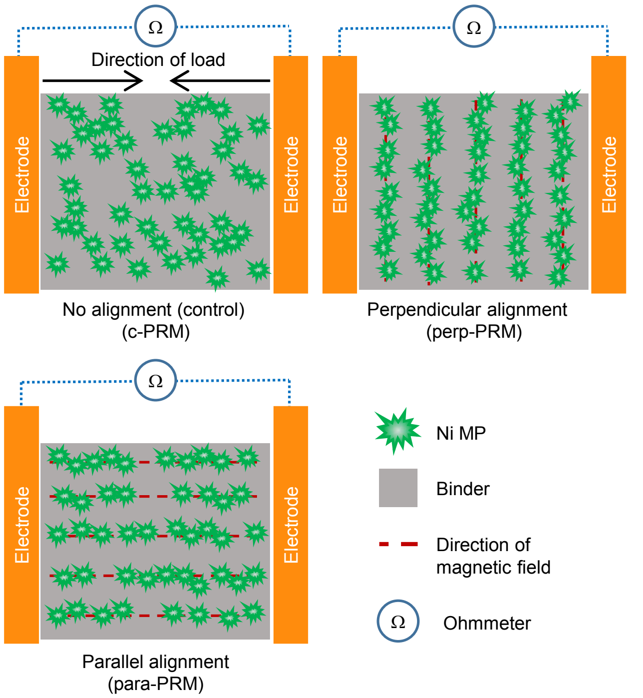

**Fig. 4** Schematic illustrations of the three different types of PRM prepared. The red dotted line indicates the direction of the magnetic field that was present during the sample preparation.

We prepared three different types of samples as depicted in Fig. 4. Resistivity of the samples were measured using two parallel electrodes that sandwiched the opposing sides of the sample. c-PRM is the sample prepared without application of magnetic field. perp-PRM and para-PRM denotes the samples with Ni MP alignment perpendicular and parallel to the direction of applied load, respectively. The differences in alignment and interparticle distance of the Ni MPs are expected to affect their percolation threshold, piezoresistive sensitivity and dynamic sensing range, as discussed in detail below.

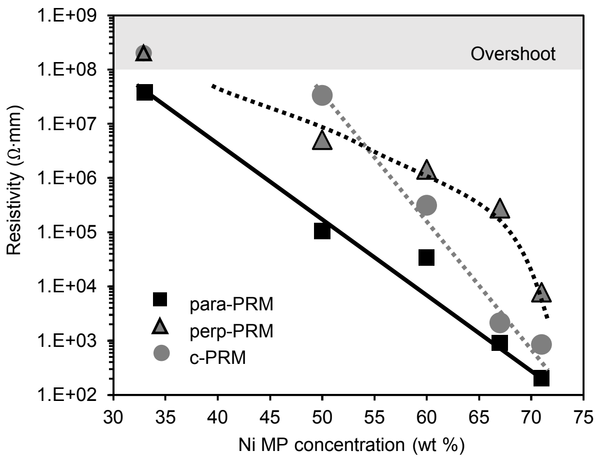

**Fig. 5** Effect of Ni MP alignment and composition on the native resistivity (zero load) of PRM. The lines are given to guide the eye and highlight the trend. Resistivity above 100 MΩ·mm was beyond the measurable range (overshoot) of the multimeter used.

### Percolation threshold

The differences in the percolation threshold with Ni MP alignment was studied by measuring the native resistivity (*i.e.*, the resistivity at zero load) of each sample (Fig. 5). In general, when the mass fraction of the Ni MPs was 33 wt %, we observed high or immeasurable resistivity ($\geq$ 100 MΩ · mm). The resistivity of CMC/SBR composite without Ni MPs was also immeasurable, which indicates that at low particle concentration, the conductive Ni MPs were well isolated from each other by the insulating CMC/SBR binder. However, with increasing fraction of the Ni MP, resistivity dropped by 3 to 5 orders of magnitude (note that the resistivity is plotted in log scale). This trend is similar to what has been reported for similar particle-based PRMs, indicating that the number of contacts between the Ni MPs increases rapidly with increasing Ni MP content.[40] This leads to more electrical pathways, and hence lower native resistivity of the PRM.

Figure 5 also highlights the effect of Ni MP alignment on the native resistivity of the samples. para-PRM has linear particle-aggregates aligned with its ends facing the electrode (Fig. 4), which enables electrical pathways to form between the two electrodes with lower particle fraction.[34, 37] Indeed, within the range of the Ni MP concentration studied here, para-PRM consistently resulted in the lowest resistivity indicating that the parallel alignment is preferable to obtain PRM with minimal Ni MP loading. This is an important merit of the Ni MP alignment, especially when it is necessary to make the PRM a lighter material. The apparent linearity of the plot can be related to the increase in electron tunnelling probability with higher Ni MP concentration (*i.e.,* reduced interparticle distance).[21] On the other hand, formation of electrical pathway between the two electrodes would be inhibited by the perpendicular alignment in perp-PRM. This is expected to result in a higher resistivity, which is the trend we observed for Ni MP content higher than 50 wt %. Similar effects of conductive particle alignment and resistivity has been reported for other composite PRMs.[25, 27] Taking the relationship between $f_m$ and $f_v$ into account (Table 1), we see from Fig. 5 that the volumetric percolation threshold are 4, 8, and 11 vol % for para-PRM, c-PRM and perp-PRM, respectively. These values are comparable to what has been reported previously for composite PRMs (1–25 vol %).[27, 34, 39, 41] This indicates that the non-uniform, porous nature of the CMC/SBR binder does not significantly affect the percolation threshold of our PRM samples.

### Piezoresistivity

Piezoresistance of the composite PRMs prepared here is gained by applying unidirectional compressive force normal to the surface of the two electrodes (see Fig. 4). This brings the conductive particles together and develops a network of electronic pathways, *i.e.,* a conducting backbone, by formation of electron tunnelling pathways or by formation of direct contact between the microparticles.[21, 39] Larger compressive force results in more pathways and hence lower resistance. Sharp protrusions of the conducting particles, such as those observed in Fig. 3, have been reported to enhance the formation of electron tunnelling pathways between microparticles.[21, 39] However, it is important to note that due to the Poisson effect, the binder material will also expand in the direction perpendicular to the direction of compression, which will pull the particles apart.[21] Hence a 3-dimensional redistribution of the particles is expected to occur, and the piezoresistive property we observe will be a result of the combination of both increase and decrease in the inter-particle distance.

Figure 6a shows the change in the normalized resistance with strain. Sensitivity of a PRM can be evaluated using the gauge factor, defined as the fractional change in resistance with applied strain.[42] The gauge factor is related to the slope of each curve in the Fig. 6a, and a PRM is considered to be more sensitive with larger gauge factor. The c-PRM showed a gradual drop in resistance with strain, starting around a strain value of 0.12. Using the approach by Abyaneh *et al.*, the gauge factor of c-PRM was −0.06.[36, 42] Significant fluctuations in the resistance were observed in this sensing regime. Such fluctuations have also been reported by other groups, and can be attributed to the inhomogeneous, random distributions of the Ni MPs, and their 3-dimensional redistribution with compression, as discussed above.[39, 40]

A steep drop in resistance with strain is seen for the para-PRM sample, starting around 0.09 strain. This indicates a rapid formation of electron pathway with compressive force. The smaller fluctuation observed within the sensing range can be attributed to the effective formation of electron pathways, both laterally and vertically with respect to the direction of the applied strain. The gauge factor for para-PRM was 23, which is comparable to the values of 10–34 reported for PRM with metal particles (Ni, Au, Cu, Zn) embedded in polydimethylsiloxane.[36, 42, 43] It is important to note that these gauge factors reported previously were obtained using randomly distributed particle with concentrations varying from 50 wt % to 88 wt %, which is much higher than the value used

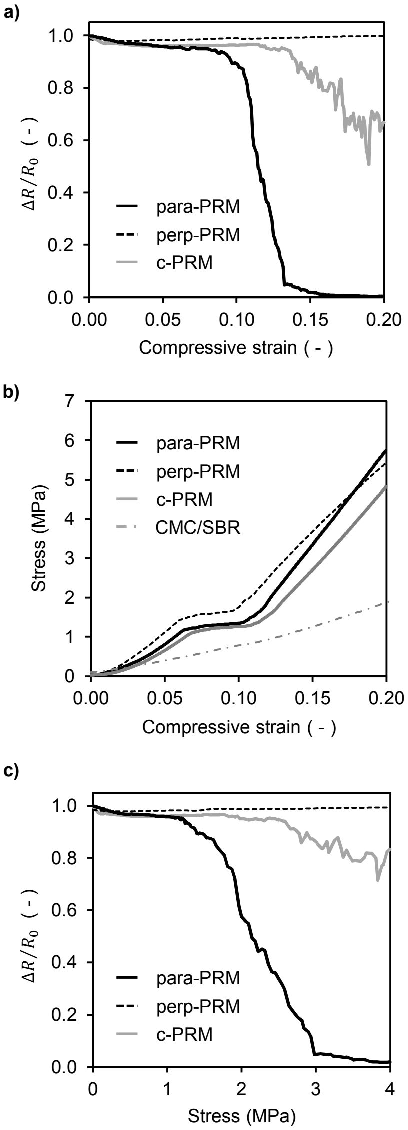

**Fig. 6** (a) Change in normalized resistance ($\Delta R/R_0$) with applied compressive strain. (b) Change in stress with applied compressive strain. (c) Change in normalized resistance ($\Delta R/R_0$) with stress obtained from Fig.6a and 6b. All PRM samples contained 33 wt % of Ni MPs.

here (33 wt %). This supports our argument that alignment of conductive particles results in higher gauge factors with lower particle concentration. Little change in normalized resistance was observed once the normalized resistance reached 0.01, indicating that particle rearrangements still occur to accommodate strain, but does not induce measurable changes in electron pathway formation/destruction.[25] No piezoresistive response was observed from perp-PRM within the 0.2 strain studied here.

In summary, the sensitivity and the dynamic sensing range were para-PRM > c-PRM > perp-PRM and 0.10–0.13 (para-PRM), ≥ 0.13 (c-PRM), N/A (perp-PRM), respectively. Such differences were expected, taking into consideration that the composition used here (33 wt % Ni) was closest to the percolation threshold of para-PRM, and furthest from that of perp-PRM. Figure 6a confirms that sensitivity and the dynamic ranges of PRM can be tuned by simply altering the direction of the anisotropic alignment and keeping all other parameters the same. Although not investigated here, intermediate responses may be obtained by aligning the particles at varying angles with respect to the applied force.

### Stress-Strain curve

All PRM samples exhibited the typical three compression regimes seen in porous structures: an initial elastic regime, a stress plateau, and a final densification regime (Fig. 6b).[44] The initial regime is due to the elastic bending of the material, and occurred between 0 and 0.06 strain. All samples exhibited larger slope in this regime compared to the CMC/SBR binder, indicating the stiffening of the material with the addition of Ni MPs. The subsequent stress plateau is generally attributed to elastic buckling, plastic yielding and/or brittle fracture of the material, due to collapsing of the porous structure. Such a regime was not observed from the CMC/SBR binder sample, suggesting that the addition of Ni MPs enhances the formation of pores within the composite. Increased porosity with addition of filler particles has been previously described for compound materials, and is attributed to the weak bonding between the filler particles and the surrounding matrix.[45] Comparing the data for para-PRM in Fig. 6a and 6b, we see that the start of the stress plateau at 0.06 strain is accompanied by the sharp drop in its relative resistance. This suggests that the stress plateau is strongly related to the initiation of electron pathways formation for materials close to its percolation threshold. The change in resistance of para-PRM continues beyond the stress plateau and into the succeeding densification regime. The final densification regime corresponds to the compression of the material after the pores have completely collapsed, and this is where the significant drop in resistance for c-PRM was observed. para-PRM exhibits a larger slope in this regime than those of c-PRM and perp-PRM. This indicates that once the pores are collapsed, the samples are stiffer along the direction of the Ni MP alignment.

### Resistance-stress curve

The stress-strain curve of our samples was measured simultaneously with the piezoresistance using the custom MTS setup (Fig. 1). Combining the data from Fig. 6a and 6b, we obtain the resistance-stress curve (Fig. 6c). This figure illustrates the range of stress that the samples are able to detect in terms of relative resistance, and also acts as a calibration curve to determine the applied compressive stress from the measured relative resistance. Defining the sensitivity to stress here as the slope of the curves in Fig. 6c, we observe that the PRM samples a trend similar to that found in the

Table 2 Compressive strain and formation potential for reported $Li_xSn_y$ phases.

| Phase | Volume increase factor[46] (-) | Uniaxial expansion factor (-) | Compressive strain on PRM* (-) |
|---|---|---|---|
| **Sn** | 1 | 1.00 | 0 |
| **$Li_2Sn_5$** | 1.23 | 1.07 | 0.018 |
| **LiSn** | 1.53 | 1.15 | 0.038 |
| **$Li_7Sn_3$** | 2.28 | 1.32 | 0.079 |
| **$Li_5Sn_2$** | 2.76 | 1.40 | 0.101 |
| **$Li_{13}Sn_5$** | 2.81 | 1.41 | 0.103 |
| **$Li_7Sn_2$** | 2.99 | 1.44 | 0.110 |
| **$Li_{22}Sn_5$** | 3.59 | 1.53 | 0.133 |

* Compressive strain was calculated assuming 8-mm thick PRM and 2-mm thick Sn foil.

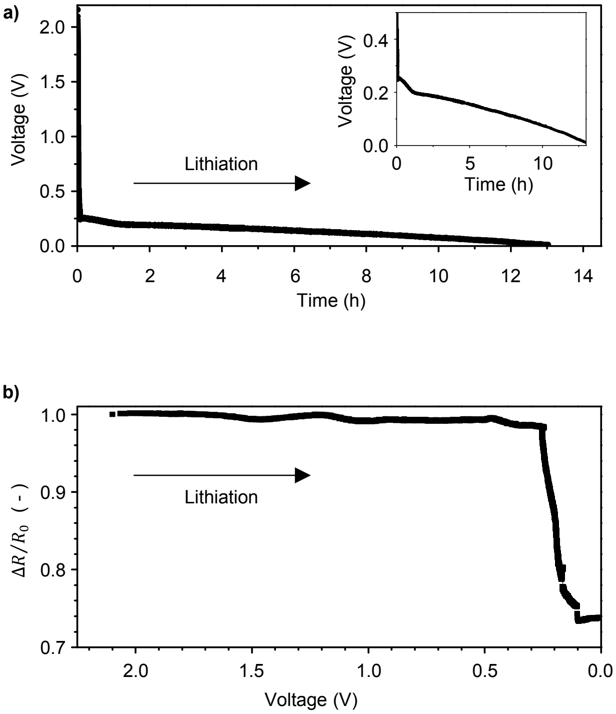

**Fig. 7** Change in (a) voltage with time and (b) normalized resistance ($\Delta R/R_0$) of para-PRM with cell voltage during lithiation of Sn. The inset is a zoomed-in figure of the voltage-time curve. The applied current density was 0.5 mA/g Sn and the cut-off voltage was 0.01 V.

piezoresistance performance: the para-PRM is most sensitive to stress between 1.2 to 3.0 MPa, the c-PRM detected stress at or above 1.9 MPa and the para-PRM did not show any sensitivity to stress in the measured range.

### ***In situ*** **strain measurement**

The lithiation of Sn to its alloying limit of $Li_{22}Sn_5$ will result in the maximum possible lithiation-induced volume change; an expansion by a factor of 3.59.[46] Recalculating the value assuming isotropic expansion in Cartesian coordinates gives a maximum uniaxial expansion factor of 1.5. Table 2 summarizes these values for various $Li_xSn_y$ phases reported in literature. In our experimental setup, with 8-mm thick PRM and 2-mm thick Sn foil, the expected maximum compressive strain of 0.13 occurs when Sn fully lithiates to $Li_{22}Sn_5$. The highest piezoresistance sensitivity at or below strains of 0.13 was observed with para-PRM, and hence this alignment was chosen for all strain-testing experiments discussed below. It is also important to note that our para-PRM cannot detect strains below 0.09 (Fig. 6a). Therefore we do not expect to detect strains due to the formation of $Li_2Sn_5$, LiSn and $Li_7Sn_3$. This limitation can be circumvented by using PRMs with wider dynamic sensing range, or by layering PRMs that function under different ranges of strains.

Our PRM samples are compatible with the low operating potential and the organic Li-ion electrolyte, since all components are materials commonly used as current collectors (Ni) or binders (CMC, SBR) in Li-ion batteries.[47-49] Hence para-PRM was used without additional treatment. Figure 7a shows the change in cell voltage as the Sn is lithiated into various $Li_xSn_y$ compounds. As seen in the inset, a rapid drop in voltage is observed until a slope starts around 0.25 V. From here, the voltage gradually decreases until it reaches its cut-off voltage of 0.01 V. The slope at 0.25 V indicates the lithiation of Sn, and the gradual decrease in voltage with time has been attributed to the continuous lithiation of Sn through different $Li_xSn_y$ phases.[50] Fig. 7b shows the change in $\Delta R/R_0$ with the cell voltage. Between the open circuit and 0.25 V, where no lithiation of Sn was indicated in Fig. 7a, minimal change in $\Delta R/R_0$ was observed. In contrast, $\Delta R/R_0$ drops rapidly between 0.25 V and 0.17 V, indicating formation of $Li_xSn_y$ leading to detectable compressive strain. Beyond 0.17 V, the drop becomes gradual again until the cell reaches 0.01 V. In summary, we show here that a simple PRM setup based on generic Li-ion battery components can act as an effective strain sensor that detects the lithiation of the active electrode and the strain it induces on the cell system.

The final $\Delta R/R_0$ value of 0.73 corresponds to a compressive strain of 0.11 (Fig. 6a). This is 15% lower than the 0.13 calculated for $Li_{22}Sn_5$, indicating that some fraction of Sn did not fully lithiate to $Li_{22}Sn_5$. Indeed, X-ray diffraction of the Sn after charging showed multiple peaks that indicated existence of Sn and multiple $Sn_xLi_y$ phases.[36] It is also possible that other components of the cell device (*e.g.*, the PC separator and Li foil) partially buffered the strain induced by Sn lithiation. A $\Delta R/R_0$ value of 0.73 also corresponds to compressive stress of 1.32 MPa. From Fig. 6b, the elastic regime of para-PRM is below 1.1 MPa. This suggests that compression due to lithiation has led to plastic deformation of our sample, and indeed we observed decrease in piezoresistive response when Sn lithiation/delithiation was repeated. The key strategy for designing a reversible PRM device to monitor extended cycling of Sn electrode would be to increase the elastic regime of the PRM, or decrease the compressive strain induced by the electrode. Elastic regime of the PRM can be extended by optimizing the porosity of the binder,[51] or by applying a binder that is more elastic than the CMC/SBR combination. The compressive strain can easily be reduced by using a thinner electrode.

## Conclusions

In conclusion, we demonstrate the first example of detecting lithiation-induced strain using composite piezoresistive materials. The piezoresistive materials were prepared from elements conventionally used in Li-ion batteries; Ni, CMC and SBR. We show that the Ni MPs can be magnetically aligned within the CMC/SBR binder to change its percolation threshold, which led to a difference in the gauge factor by three orders of magnitude. The magnetic alignment of the conductive Ni MPs was used to tune the sensitivity and the dynamic sensing range of the PRM and effectively detect strain induced by Sn lithiation. The method described here offers significant merits over conventional approaches: the ability to directly monitor strain without complex modelling, the simple low cost setup that does not require specialized equipment, and the ability to easily control the PRM performance by magnetically directed assembly. We are interested in expanding this research to explore other Li-ion battery materials for PRM preparation, and study the effect of microparticle shape and dimensions to improve PRM performance.

## Acknowledgements

We thank Christine Pratt for her support and help with the MTS/resistance experiment, Professor Wyatt Tenhaeff for access to the digital bench-top multimeter, Brian McIntyre and the Integrated Nanosystems Center for use of FE-SEM, John Miller and the River Campus Instrument Machine Shop for consultation and fabrication of the custom devices. We also acknowledge Professor David J. Quesnel and Professor Wyatt Tenhaeff for their expertise and insightful discussions. This work has been funded by the Department of Chemical Engineering at the University of Rochester.

## Notes

[a] Department of Chemical Engineering, University of Rochester, USA. Email: hitomi.mukaibo@rochester.edu

[b] Materials Science Program, University of Rochester, USA.

† Electronic Supplementary Information (ESI) available. See DOI: 10.1039/b000000x/

## References

1 V. Etacheri, R. Marom, R. Elazari, G. Salitra and D. Aurbach, *Energy Environ. Sci.*, 2011, **4**, 3243-3262.

2 P. G. Bruce, B. Scrosati and J.-M. Tarascon, *Angew. Chem., Int. Ed.*, 2008, **47**, 2930-2946.

3 W. J. Zhang, *J. Power Sources*, 2011, **196**, 13-24.

4 A. Mukhopadhyay and B. W. Sheldon, *Prog. Mater. Sci.*, 2014, **63**, 58-116.

5 E. M. C. Jones, M. N. Silberstein, S. R. White and N. R. Sottos, *Exp. Mech.*, 2014, **54**, 971-985.

6 Y. Qi and S. J. Harris, *J. Electrochem. Soc.*, 2010, **157**, A741-A747.

7 P. K. Leung, C. Moreno, I. Masters, S. Hazra, B. Conde, M. R. Mohamed, R. J. Dashwood and R. Bhagat, *J. Power Sources*, 2014, **271**, 82-86.

8 J. Chen, A. K. Thapa and T. A. Berfield, *J. Power Sources*, 2014, **271**, 406-413.

9 T. Ohzuku, N. Matoba and K. Sawai, *J. Power Sources*, 2001, **97-98**, 73-77.

10 T. Kim, S. Park and S. M. Oh, *J. Electrochem. Soc.*, 2007, **154**, A1112-A1117.

11 M. Winter, G. H. Wrodnigg, J. O. Besenhard, W. Biberacher and P. Novak, *J. Electrochem. Soc.*, 2000, **147**, 2427-2431.

12 S. Kalinin, N. Balke, S. Jesse, A. Tselev, A. Kumar, T. M. Arruda, S. Guo and R. Proksch, *Mater. Today*, 2011, **14**, 548-558.

13 L. Y. Beaulieu, T. D. Hatchard, A. Bonakdarpour, M. D. Fleischauer and J. R. Dahn, *J. Electrochem. Soc.*, 2003, **150**, A1457-A1464.

14 A. Timmons and J. R. Dahn, *J. Electrochem. Soc.*, 2007, **154**, A444-A448.

15 C. R. Becker, K. E. Strawhecker, Q. P. McAllister and C. A. Lundgren, *ACS Nano*, 2013, **7**, 9173-9182.

16 L. Y. Beaulieu, K. W. Eberman, R. L. Turner, L. J. Krause and J. R. Dahn, *Electrochem. Solid-State Lett.*, 2001, **4**, A137-A140.

17 J. Y. Huang, L. Zhong, C. M. Wang, J. P. Sullivan, W. Xu, L. Q. Zhang, S. X. Mao, N. S. Hudak, X. H. Liu, A. Subramanian, H. Y. Fan, L. A. Qi, A. Kushima and J. Li, *Science*, 2010, **330**, 1515-1520.

18 X. H. Liu, H. Zheng, L. Zhong, S. Huang, K. Karki, L. Q. Zhang, Y. Liu, A. Kushima, W. T. Liang, J. W. Wang, J.-H. Cho, E. Epstein, S. A. Dayeh, S. T. Picraux, T. Zhu, J. Li, J. P. Sullivan, J. Cumings, C. Wang, S. X. Mao, Z. Z. Ye, S. Zhang and J. Y. Huang, *Nano Lett.*, 2011, **11**, 3312-3318.

19 J. M. Yuk, H. K. Seo, J. W. Choi and J. Y. Lee, *ACS Nano*, 2014, **8**, 7478-7485.

20 S.-C. Chao, Y.-C. Yen, Y.-F. Song, Y.-M. Chen, H.-C. Wu and N.-L. Wu, *Electrochem. Commun.*, 2010, **12**, 234-237.

21 S. Stassi, V. Cauda, G. Canavese and C. F. Pirri, *Sensors*, 2014, **14**, 5296-5332, 5237.

22 D. S. McLachlan, M. Blaszkiewicz and R. E. Newnham, *J. Am. Ceram. Soc.*, 1990, **73**, 2187-2203.

23 R. A. Landa, P. Soledad Antonel, M. M. Ruiz, O. E. Perez, A. Butera, G. Jorge, C. L. P. Oliveira and R. M. Negri, *J. Appl. Phys.*, 2013, **114**, 213912/213911-213912/213911.

24 M. R. Jolly, J. D. Carlson and B. C. Munoz, *Smart Mater. Struct.*, 1996, **5**, 607-614.

25 N. Kchit and G. Bossis, *J. Phys.: Condens. Matter*, 2008, **20**, 204136/204131-204136/204135.

26 S. Kim, J. Byun, S. Choi, D. Kim, T. Kim, S. Chung and Y. Hong, *Adv. Mater.*, 2014, **26**, 3094-3099.

27 M. Knaapila, H. Hoeyer, J. Kjelstrup-Hansen and G. Helgesen, *ACS Appl. Mater. Interfaces*, 2014, **6**, 3469-3476.

28 E. Sancaktar and N. Dilsiz, *J. Adhes. Sci. Technol.*, 1997, **11**, 155-166.

29 T. M. Johnson, D. T. Fullwood and G. Hansen, *Compos. Part B-Eng.*, 2012, **43**, 1155-1163.

30 R. A. Vaia and J. F. Maguire, *Chem. Mater.*, 2007, **19**, 2736-2751.

31 Y. Kim, J. Zhu, B. Yeom, P. M. Di, X. Su, J.-G. Kim, S. J. Yoo, C. Uher and N. A. Kotov, *Nature*, 2013, **500**, 59-63.

32 H. Hoyer, M. Knaapila, J. Kjelstrup-Hansen, X. Liu and G. Helgesen, *J. Polym. Sci., Part B: Polym. Phys.*, 2012, **50**, 477-483.

33 J. Seo, T. J. Lee, C. Lim, S. Lee, C. Rui, D. Ann, S.-B. Lee and H. Lee, *Small*, 2015, DOI: 10.1002/smll.201401812.

34 J. E. Martin, R. A. Anderson, J. Odinek, D. Adolf and J. Williamson, *Phys. Rev. B: Condens. Matter Mater. Phys.*, 2003, **67**, 094207/094201-094207/094211.

35 CRC Handbook of Chemistry and Physics, http://www.hbcpnetbase.com, (accessed February 24 2015).

36 *See the Supporting Information for details*.

37 W. Li, L. Yu, Y. Zhu and D. Hua, *J. Phys. Chem. C*, 2010, **114**, 14004-14007.

38 J. Kuusipalo, A. M. Savijaervi, S. Norval, M. J. Adlen and D. H. Mackerron, *J. Mater. Sci.*, 2004, **39**, 6909-6919.

39 D. Bloor, K. Donnelly, P. J. Hands, P. Laughlin and D. Lussey, *J. Phys. D: Appl. Phys.*, 2005, **38**, 2851-2860.

40 G. Canavese, S. Stassi, M. Stralla, C. Bignardi and C. F. Pirri, *Sensor Actuat. A-Phys*, 2012, **186**, 191-197.

41 T. Nagai, N. Aoki, Y. Ochiai and K. Hoshino, *ACS Appl. Mater. Interfaces*, 2011, **3**, 2341-2348.

42 M. K. Abyaneh and S. K. Kulkarni, *J. Phys. D: Appl. Phys.*, 2008, **41**, 135405/135401-135405/135407.

43 S. Stassi, G. Canavese, V. Cauda, S. L. Marasso and C. F. Pirri, *Nanoscale Res. Lett.*, 2012, **7**, 327, 325 pp.

44 L. J. Gibson, *Mater. Sci. Eng., A*, 1989, **A110**, 1-36.

45 D. D. L. Chung, in *Composite Materials: Science and Applications*, Springer, London, 2nd edn., 2010, ch. 6, pp. 192-194.

46 I. A. Courtney and J. R. Dahn, *J. Electrochem. Soc.*, 1997, **144**, 2045-2052.

47 Y. Xu, L. Fei, E. Fu, B. Yuan, J. Hill, Y. Chen, S. Deng, P. Andersen, Y. Wang and H. Luo, *J. Power Sources*, 2013, **242**, 604-609.

48 J.-P. Yen, C.-M. Lee, T.-L. Wu, H.-C. Wu, C.-Y. Su, N.-L. Wu and J.-L. Hong, *ECS Electrochem. Lett.*, 2012, **1**, A80-A82.

49 W.-R. Liu, M.-H. Yang, H.-C. Wu, S. M. Chiao and N.-L. Wu, *Electrochem. Solid-State Lett.*, 2005, **8**, A100-A103.

50 M. Winter and J. O. Besenhard, *Electrochim. Acta*, 1999, **45**, 31-50.

51 T. Zhai, D. Li, G. Fei and H. Xia, *Compos. Part A-Appl. S.*, 2015, **72**, 108-114.